Article

Photocorrosion Suppression of ZnO Nanoparticles via Hybridization with Graphite-like Carbon and Enhanced Photocatalytic Activity

Liwu Zhang, Hanyun Cheng, Ruilong Zong, and Yongfa Zhu

J. Phys. Chem. C, **2009**, 113 (6), 2368-2374• DOI: 10.1021/jp807778r • Publication Date (Web): 21 January 2009

Photocorrosion Suppression of ZnO Nanoparticles via Hybridization with Graphite-like Carbon and Enhanced Photocatalytic Activity

Liwu Zhang, Hanyun Cheng, Ruilong Zong, and Yongfa Zhu*

Department of Chemistry, Tsinghua University, Beijing 100084, People's Republic of China

Received: September 2, 2008; Revised Manuscript Received: December 11, 2008

A method to suppress the photocorrosion of ZnO nanoparticles was developed by surface hybridization of ZnO with graphite-like carbon layers. The presence of carbon on the surface of the ZnO could significantly suppress the coalescence and crystal growth of ZnO nanoparticles during high-temperature treatment. The nanosized structure of ZnO was well preserved even after high-temperature calcination. The photocatalytic activity of ZnO was enhanced by hybridization with carbon layers attributed to the improved adsorption ability and crystallinity. The as-prepared samples exhibited high activity even after 720 h of photocatalysis reaction, while the pure ZnO nanoparticle was almost deactivated in 100 h due to serious photocorrosion. The as-prepared samples also showed much better activity under extreme pH conditions than that of pure ZnO. The mechanism of photocorrosion suppression and higher stability was then systematically investigated based on the crystal structure and the photocatalysis degradation process.

1. Introduction

In recent years, semiconductor photocatalysis has become more and more attractive and important since it has a great potential to contribute to environmental remediation. One of the most important aspects of photocatalysis is the selection of semiconductor materials like ZnO and TiO_2, which are close to being two of the ideal photocatalysts. They are relatively inexpensive, and they provide photogenerated holes with high oxidizing power due to their wide band gap energy.[1,2]

As a well-known photocatalyst, ZnO has received much attention in the decomposition and complete mineralization of environmental pollutants.[3−7] Some studies have confirmed that ZnO exhibits a better efficiency than TiO_2 in photocatalytic degradation of some dyes in aqueous solution.[8,9] Furthermore, the emitting properties of ZnO have been made possible to set up an original catalytic system able to "sense and shoot" environmental contaminants,[10] thus motivating further exploration of the properties of this oxide. Unfortunately, the photocorrosion of ZnO that occurs with the UV light irradiation, as well as the susceptibility of ZnO to facile dissolution at extreme pH values, have significantly decreased the photocatalytic activity of ZnO in aqueous solution and blocked the application of ZnO in photocatalysis.[11−17] It is anticipated that ZnO could become an excellent photocatalyst if the photocorrosion and susceptibility can be improved or suppressed. However, few studies have focused on this topic. It has been reported by Comparelli et al. that surface organic coating of ZnO nanocrystals could provide the oxide with resistance to photocorrosion and pH variation.[18] Stable ZnO photocatalyst was also obtained by embedding in perfluorinated ionomer membranes.[15] Thus it can be seen that a suitable protection of the catalyst surface could significantly improve the stability of ZnO. It has been demonstrated that surface coating of TiO_2 with carbon could efficiently improve the photocatalytic activity, and protect TiO_2 from phase transformation under high temperature.[19−21] The present work explores further this topic considering the case of ZnO. Although preparation of carbon modified ZnO and enhanced photocatalytic activity have been reported,[22,23] little attention was paid to the synergic effect between graphitic carbon and ZnO. Herein, we present a simple method to hybrid ZnO with graphite-like carbon layers, and first demonstrate the role of the carbon layer in the protection of ZnO against photocorrosion. The synergic effect between ZnO and graphite-like carbon and the resulting impact on the photocatalytic activity were then investigated systematically.

1. Experiment Section

2.1. Synthesis of the ZnO/Carbon Nanoparticles. Particulate ZnO (particle diameter 10−20 nm, surface area 57.3 $m^2\ g^{-1}$) was commercially available. All the other reactants used in the experiments were of analytic purity, bought from the Beijing Chemical Reagent Factory and used without further purification. The preparation of graphite-like carbon hybridized ZnO was realized by two steps. First, 0.4 g of ZnO and 0.5 g of glucose were dissolved in 35 mL of water to form a clear solution with the assistance of ultrasonication. The solution was then transferred into a 40 mL autoclave and hydrothermally treated at 180 °C for 4 h. The pure products were obtained after centrifugation at 5000 rpm for 20 min. A clean process involving five cycles of centrifugation/wash/redispersion was repeated in water. The samples were then dried in an oven at 80 °C for 4 h. According to repeated experimental results, the samples obtained have a ZnO@C core−shell structure, and the shell thickness depended on the amount of glucose used. The graphitization process was conducted in a tube furnace by calcining at 800 °C for 3 h in flowing N_2 with a rate of 60 mL min^{-1}.

In this paper, the products were named in the following way: the products prepared with different mix ratios of glucose (0.5 g, 0.6 g, 0.7 g, 0.8 g, 1.0 g, 1.5 g), and followed by calcining at 800 °C, were named as GZ05, GZ06, GZ07, GZ08, GZ10, and GZ15, respectively.

2.2. Analysis Techniques. High resolution transmission electron microscopy (HRTEM) images were obtained with a JEM 2010F field emission transmission electron microscope with an accelerating voltage of 200 kV. X-ray diffraction (XRD)

* To whom correspondence should be addressed. Phone: +86-10-62783586. Fax: +86-10-62787601. E-mail: zhuyf@tsinghua.edu.cn.

10.1021/jp807778r CCC: $40.75
Published on Web 01/21/2009

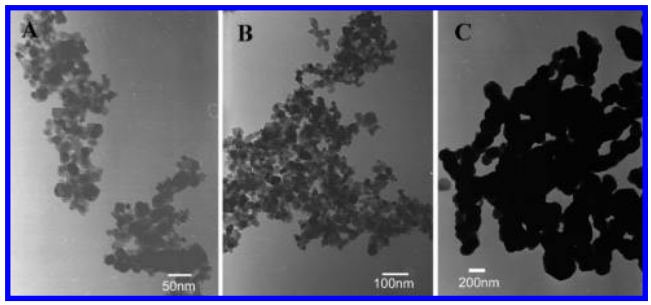

Figure 1. TEM images of ZnO and GZ composite: (A) ZnO, (B) GZ07, and (C) ZnO calcined at 800 °C without carbon coating.

experiments were carried out with a Rigaku DMAX-2400 diffractometer with Cu Kα radiation. The average crystal size was determined from XRD pattern parameters according to the Scherrer equation: $D_c = K\lambda/(\beta \cos \theta)$, where D_c is the average crystal size, K is the Scherrer constant equal to 0.89, β is the full width at half-maximum (fwhm), and θ is the diffraction angle. The grain size was measured with a Hitachi H-800 transmission electron microscope (TEM). The accelerating voltage of the electron beam was 200 kV. Raman spectra were acquired with a Raman microspectrometer (Renishaw 1000 NR), using an Ar ion laser (632.8 nm). Raman spectra were measured under a microscope, using a 20 objective to focus the incident excitation laser radiation into a spot 1−2 or 2−3 μm in diameter to collect the scattered light. The laser power was kept low enough to avoid heating of the samples by optical filtering and/or defocusing of the laser beam at the sample surface. Spectra were collected in the range of 2000−200 cm^{-1} with a resolution of 1 cm^{-1}. UV−vis diffuse reflectance spectra (DRS) of the samples were measured by using a Hitachi U-3010 UV−vis spectrophotometer. TGA-DTA analyses were performed on a Dupont 1090 thermal analyzer, the atmosphere was air, and the heating rate was 5 deg/min.

2.3. Photochemical Experiments. The photocatalytic activities of the as-prepared samples for the degradation of MB in solution were tested under UV light. An 8 W UV lamp (λ = 254 nm, the Institute of Electric Light Source, Beijing) was used as the light resource, and the average light intensity was 150 $\mu W \cdot cm^{-2}$. A 100 mg sample was dispersed in a 100 mL MB suspension (1×10^{-5} M). Prior to the irradiation, the suspensions were magnetically stirred in the dark for 0.5 h to reach the absorption−desorption equilibrium. The suspensions were kept under constant air-equilibrated conditions before and during the irradiation. At given time intervals, 3 mL of the aliquots was sampled, and centrifugated to remove the particles. The filtrates were analyzed by recording variations in the absorption band (665 nm) in the UV−visible spectra of MB with a Hitachi U-3010 UV−vis spectrophotometer.

3. Results and Discussion

3.1. Structure and Morphology of ZnO/Carbon Nanoparticles. In the current work, the encapsulation of ZnO with graphite-like carbon was realized by two steps. The first step is fabricating ZnO@C core−shell structure through a hydrothermal method at 180 °C, using commercial ZnO and glucose as starting materials. The shell thickness was tunable by simply increasing or decreasing the glucose content. Then, the graphitization of the carbonaceous cages was conducted in a tube furnace by calcining at 800 °C for 3 h in a N_2 gas atmosphere. Figure 1 shows the transmission electron microscopy (TEM) images of ZnO and GZ composite. It can be seen from Figure 1A that the original ZnO nanoparticles have a particle size of about 20 nm.

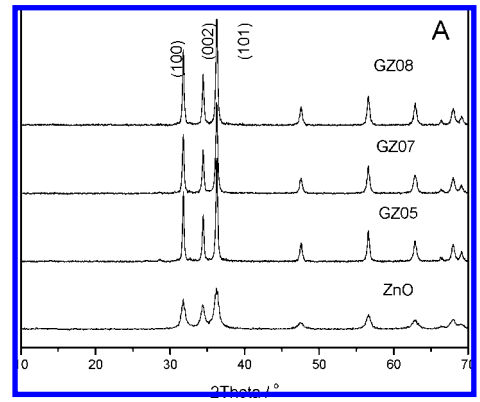

Figure 2. XRD patterns of GT products prepared with different mixing ratios of ZnO and glucose.

TABLE 1: Physicochemical Characterization of GZ and ZnO Samples

	mixing ratio of glucose (mass %)	carbon content (mass %)	carbon ($I_{D\text{-band}}/I_{G\text{-band}}$)	particle size of ZnO (nm)
ZnO	0	0		20
ZnO-800	0	0		200−400
GT05	55	10.1	1.01	∼100
GT06	60	14.2	0.94	70
GT07	64	16.9	0.83	40
GT08	66	23.6	0.85	40
GT10	72	25.6	0.84	35

Figure 1B shows the TEM image of GZ07, which is prepared with 0.7 g of glucose added. The carbon shell is not visible at this resolution, while it is clearly observed in the high-resolution TEM image (shown in Figure 4). The average particle size of GZ07 is about 40 nm, which is larger than the original ZnO nanoparticles, indicating the aggregation and growth of ZnO crystals during calcination. For comparison, a sample of ZnO without carbon coating was also prepared by direct calcination of ZnO naoparticles at 800 °C. The result is shown in Figure 1C. An intense crystal growth is observed, and the particle size is about 200−400 nm, while the sample of GZ07 has a particle size of ∼40 nm under identical experimental conditions. Obviously, the presence of carbon on the surface of the ZnO inhibits its crystal growth, leading to a higher thermal stability. The particle size of ZnO particles in the GZ samples decreased as the carbon content increased, as shown in Table 1. The carbon shells are acting as barriers for the crystal growth of ZnO. It can be speculated that the high energy introduced into the system through the high temperature is directly exposed to the carbon shells and not the ZnO core; thus, the core retains nanosized particles. In the studies on TiO_2, it is also found that

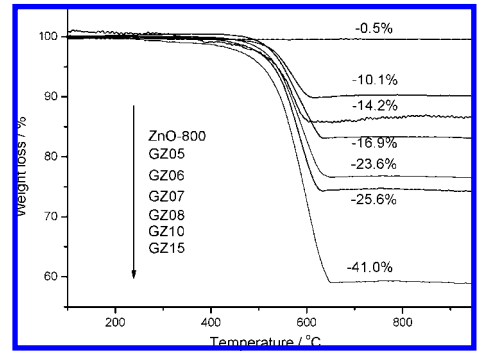

Figure 3. The TGA spectrum of GZ samples.

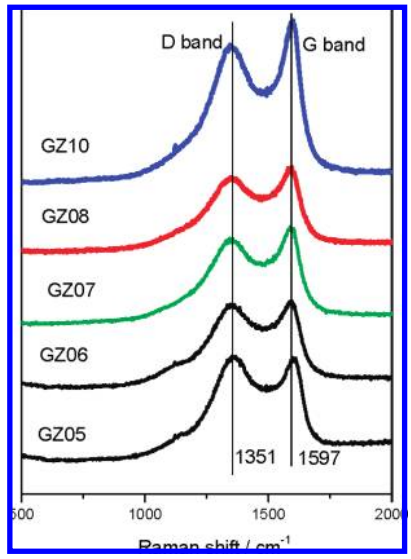

Figure 4. Raman spectra of GZ samples exhibiting graphitic modes.

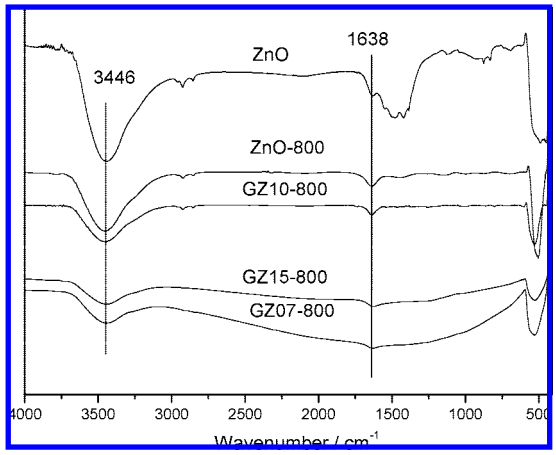

Figure 5. FT-IR spectra of GZ samples and ZnO.

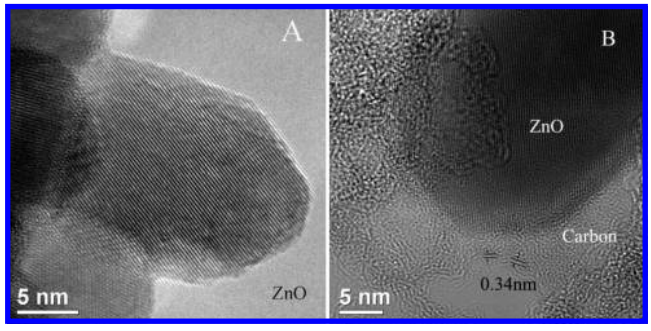

Figure 6. High-resolution (HR)-TEM images: (A) ZnO and (B) GZ07.

the carbon shell could effectively suppress the crystal growth as well as the phase transformation of TiO_2 from anatase to rutile even under high temperature.[19−21] Therefore, it is believed that carbon is a good candidate for the protection of nanoparticles against aggregation and coalescence during high-temperature treatment.

Figure 2 shows the X-ray diffraction (XRD) patterns of ZnO and GZ samples prepared with different mass ratios of glucose and ZnO. All the reflections of the samples can be exactly indexed as the zincite structure (JCPDS 89-1397). Compared with the original ZnO nanoparticle, the diffraction peaks of GZ

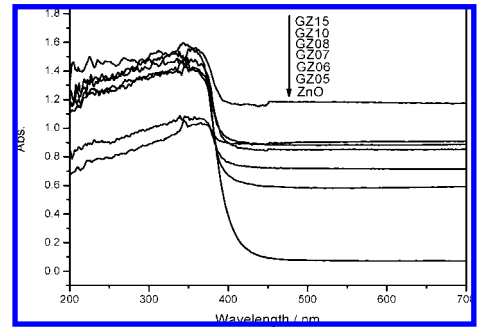

Figure 7. The UV−vis diffuse reflectance spectroscopy of ZnO and GZ samples.

samples are intensified and become sharper, suggesting that the high-temperature treatment during the graphitization process has enhanced the crystal structure of ZnO significantly. The average crystallite size for ZnO and GZ samples was determined from the line width broadening of the XRD peak corresponding to (0 0 2) reflection, using the Debye−Scherrer equation. The calculated crystallite size of the original ZnO nanoparticle is about 16 nm, while it is calculated to be about 32 nm for the GZ samples, which is in good accordance with TEM images. So, the growth of ZnO crystal in GZ samples still occurred during the high-temperature calcination; however, the presence of carbon on the surface could significantly suppress the crystal coalescence to a large extent, considering the directly calcined ZnO sample.

An estimate of the carbon content in the ZnO/carbon nanoparticles could be obtained by thermogravimetric analysis (TGA), as shown in Figure 3. For all the samples, no obvious weight loss was observed until 500 °C. Major weight loss commenced at 500 °C and was completed at 620 °C, which can be attributed to the oxidation of carbon. The carbon content of the samples increased with increasing mass ratio of glucose and ZnO during hydrothermal treatment, and is therefore easily controlled by changing the glucose mass ratio. In the present work, the carbon content of sample GZ07 was calculated to be approximately 16.9 wt %.

The nature of the carbon present in the GZ samples was also investigated by Raman spectroscopy and the results are shown in Figure 4. All sample spectra show two peaks around 1351 and 1597 cm^{-1}. The Raman-active E_{2g} mode at 1597 cm^{-1} is characteristic for graphitic sheets and we were able to record well-defined *G*-bands for all our samples, which confirms the presence of sp^2 carbon-type structures within the carbonaceous wall of the GZ samples.[24] The *D*-band at around 1341 cm^{-1} can be attributed to the presence of defects within the hexagonal graphitic structure. Since the intensities of the *G*-bands are comparable to those of the *D*-bands, we conclude that the samples have some degree of atomic scale ordering. Compared with the spectra of pure graphite crystals (1575 cm^{-1}), the *G*-band shifted to higher wavenumbers in all sample spectra, which suggests some structural imperfections of the carbon shells.[25,26] The intensity ratio of *D*- and *G*-band ($I_{D\text{-band}}/I_{G\text{-band}}$) is indicative of the degree of graphitization and its value for each sample is shown in Table 1. The ratio decreases with increasing carbon content first, indicating that samples with thicker carbon shells form a more ordered carbon structure during the graphitization process. But when the carbon content is more than GZ07, the ratio increases, suggesting the carbon structure becomes more disordered. On the basis of the result above, it is known that the degree of graphitization depended not only on the graphitization temperature but also on the mass

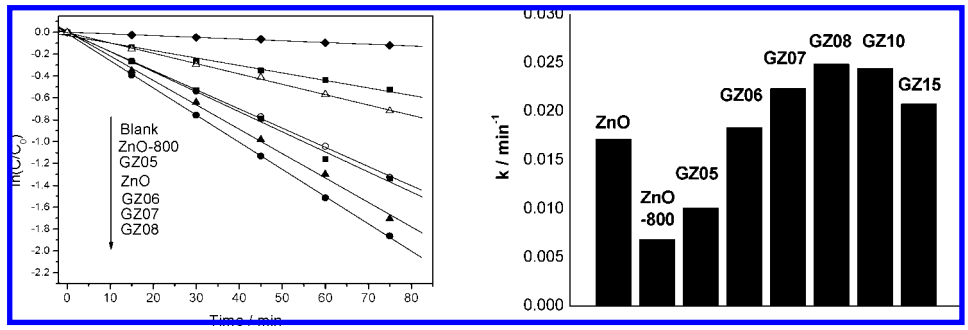

Figure 8. Photocatalytic degradation of MB over the as-prepared samples under UV-light irradiation ($\lambda = 254$ nm): catalyst loading, 0.5 g L^{-1}; MB, 1×10^{-5} M.

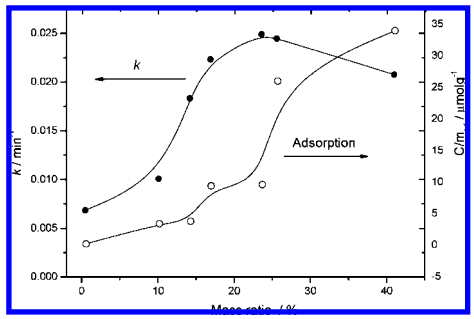

Figure 9. The curves of reaction rate constants k and adsorption ability vs glucose loading in GZ samples.

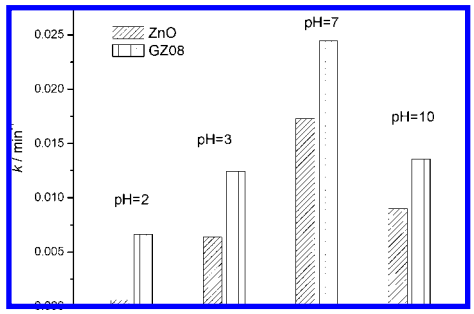

Figure 10. The photodegradation of MB in the presence of ZnO and GZ08 at different pH values.

ratio of the carbon on the surface of ZnO. The best mass ratio for graphitization of the carbon is found at 16.9 wt % (GZ07) in present work.

Figure 5 shows the FT-IR spectral analysis of the GZ samples and ZnO. The spectrum of ZnO prior to calcination shows an absorption peak at 3446 cm^{-1}, which corresponds to the O−H stretching of the surface adsorbed water molecule. The band at ~2900 cm^{-1} shows the presence of C−H species. The three bands occurring in the region of 1000−500 cm^{-1} and the one at 1380 cm^{-1} correspond to the different modes of CO_3^{2-}. However, in the case of GZ samples, the peaks corresponding to the different modes of CO_3^{2-} are no longer present and show the peak of only nanosized ZnO at ~490 cm^{-1}. It is important to note that the intensity of the absorption peak at 3446 cm^{-1} related to surface −OH of ZnO is significantly decreased in the GZ samples, which could be attributed to the surface coating with carbon layers.

Figure 6 shows high-resolution (HR) TEM images of sample GZ07 which were used to estimate carbon shell thickness and ZnO nanoparticle size. The images show that the ZnO particles are surrounded by carbon layers, and the overall thickness of the carbon shell is about 10 nm. It is observed that the d-spacing of the carbon layers is 0.34 nm, which is in agreement with the literature of graphitic layers. As can be seen from the HRTEM images as well, there are still many defects within the carbon layers, indicating a poor graphitization degree, which is in good agreement with the Raman results. However, since the surface of the ZnO nanoparticles is fully covered with a thin graphite-like carbon film a good electronic contact between oxide semiconductor and carbon was achieved.

The optical properties of the GZ samples were probed with UV−vis diffuse reflectance spectroscopy, shown in Figure 7. As expected, ZnO shows the characteristic spectrum with its fundamental absorption sharp edge rising at 410 nm, while the GZ samples absorb in the visible light region due to the presence of carbon on the ZnO surface. The absorption edge of ZnO can also be detected in the spectra of the GZ samples. The ZnO peak is not shifted for all the GZ samples, indicating identical band gap energies. In the present work, most of the carbon in the GZ samples was free, graphitic carbon, hence no change in band gap energy was observed and instead an intense, broad background absorption in the visible light region dominated the UV−vis spectra. Additionally, it is noteworthy that there is an obvious correlation between carbon content and changes observed in the UV−vis spectrum of a sample. The UV−vis absorption of the GZ samples increases with increasing carbon content. This suggests an increased electric surface charge of the oxide within the composite due to the introduction of the carbon, which can possibly cause modifications of the fundamental process of electron−hole pair formation during irradiation.

3.2. Photocatalytic Properties. The photocatalytic activities of the as-prepared samples were evaluated by the degradation of MB in aqueous solution, shown in Figure 8. The first-order linear relationship was revealed by the plots of $\ln(C/C_0)$ vs irradiation time (t). The blank test confirmed that MB was hardly degraded under UV light in the absence of the catalyst. When exposed to UV light, about 85% of MB can be photodegraded by ZnO after 75 min of irradiation. GZ08 showed the highest photocatalytic activity in the decomposition of MB, 1.5 times higher than that of the original ZnO. GZ06, GZ07, GZ10, and GZ15 also showed higher activity than that of neat ZnO, while GZ05 with less carbon exhibited decreased activity. However, all the GZ samples exhibited much higher photocatalytic activities than the ZnO-800 sample, which was prepared under identical experimental conditions with GZ samples by direct calcination of ZnO without carbon coating.

The photocatalytic activity of semiconductor oxides is mainly governed by surface area, crystallinity, adsorption ability, and so on. The particle size and adsorption ability significantly affects the photocatalytic activity of GZ samples. Figure 9 shows a relationship between the glucose loading with the adsorption ability of GZ samples and with the apparent reaction rate constant k. As the carbon loading increased, the adsorption abilities of GZ samples were significantly improved. Thus the

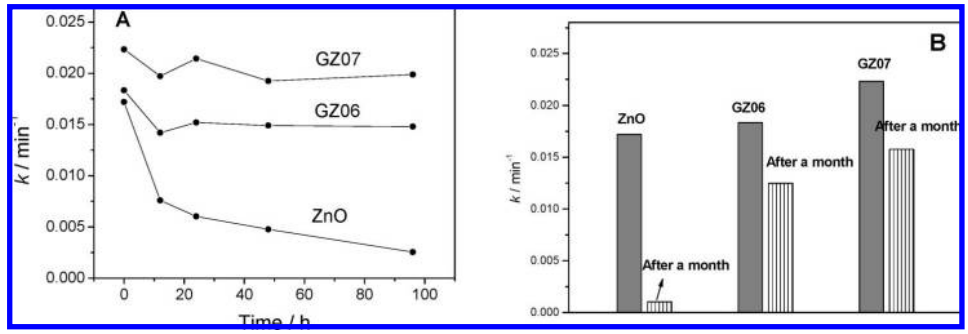

Figure 11. (A) The photostability experiment: GZ06, GZ07, and ZnO. (B) The photocatalytic action of GZ samples and ZnO before and after a month of photocatalytic reaction.

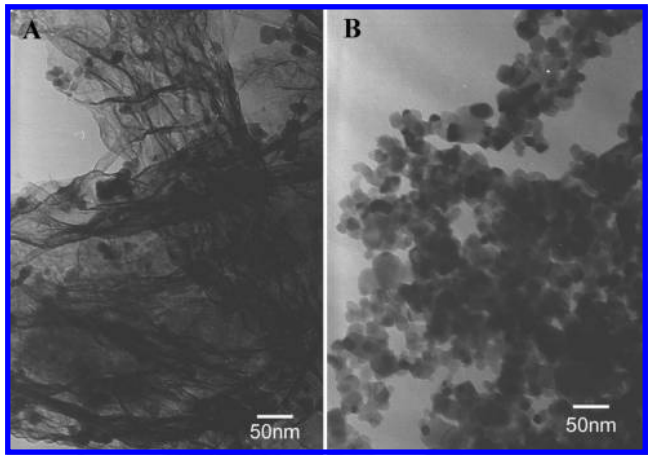

Figure 12. The TEM images of ZnO and GZ07 after photocatalysis reaction: (A) ZnO and (B) GZ07.

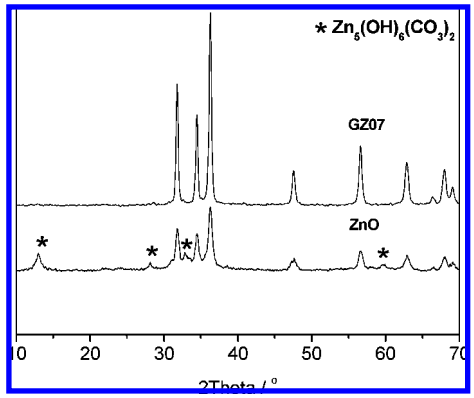

Figure 13. XRD patterns of pure ZnO and GZ07 after the photocatalysis experiment.

photocatalytic activities of the GZ samples increased with the carbon loading first, due to the enhanced adsorption ability. Notably, the GZ06 sample has comparable adsorption ability with GZ05, but the reaction rate is twice higher. This sudden increase in reaction rate is also observed in the study on TiO_2.[21] In the case of TiO_2, the transformation of anatase phase to rutile was efficiently suppressed due to the carbon coating, and the minimum amount of coated carbon for the suppression of phase transformation was found at about 5.4 wt %. Herein, the carbon coating could prevent the ZnO nanoparticles against aggregation and coalescence during high-temperature treatment. With lower carbon content, the coalescence and growth of ZnO nanoparticles was not efficiently suppressed during the graphitization process, consequently, GZ05 showed lower activity than the original ZnO and much lower activity than other GZ samples.

Interestingly, when the carbon loading is higher than that of GZ08, such as GZ10 and GZ15, where much better adsorption abilities are obtained, lower photocatalytic activities are observed. The decrease in activity with higher carbon content is considered to be related to increased absorbing and scattering of photons by surplus carbon in the photoreaction system. The coated graphite layers would shield the light reaching the surface of ZnO photocatalyst. Therefore, to get a high photodecomposition rate, a balance among these different effects of the graphite layers is required. The sample of GZ08 gave the highest rate constant in the present work, where nanosized ZnO particles are preserved, good adsorption ability is possessed, and the graphite layer is thin enough to transmit light to the surface of the ZnO particle.

3.3. Effect of pH. In Figure 10 the photodegradation of MB in the presence of ZnO and GZ08 is studied in the pH range 2−10. For both catalysts, the experimental data show a relatively higher photocatalytic rate at pH 7. Generally, the effect of pH on organics degradation assisted by the semiconductor oxides has been related to the establishment of acid−base equilibrium governing the surface chemistry of metal oxides in water. For microcrystalline ZnO, the zero point charge pH (pH_{ZPC}) is reported to be about 9.0. MB is positively charged in water and the pK_a is greater than 12. The effect of pH on the photocatalytic activities can thus be understood in terms of electrostatic interactions between MB and the catalyst surface. The attractive interaction is beneficial to increase the encounter probability of the hydroxyl radicals with MB and enhance the photocatalytic efficiency, while the repulsive interaction would hinder the overall reaction. When pH is below 12, MB is positively charged, whereas the catalysts are negatively charged above pH ~9. Therefore, in the pH range 9−12 the negatively charged ZnO and the positively charge MB should readily attract each other, while they should repulse each other when pH is below 9. As expected, the degradation rate at around pH 10 is higher than that at around pH 2 and 3. However, the optimal condition was found at around pH 7, at which the catalyst and MB are both positively charged. So, other effects that account for the relative photocatalytic behavior as a function of pH must be taken into consideration, besides the electrostatic interaction. In an acidic environment, ZnO nanoparticles exhibit a tendency to dissolve:

$$ZnO + 2H^+ \rightarrow Zn^{2+} + H_2O$$

And in an alkaline environment, ZnO can undergo dissolution according to

$$ZnO + H_2O + 2OH^- \rightarrow Zn(OH)_4^{2-}$$

At extreme pH values, such as pH 2 and 10, the ZnO nanoparticles readily dissolved. Therefore, the decreased pho-

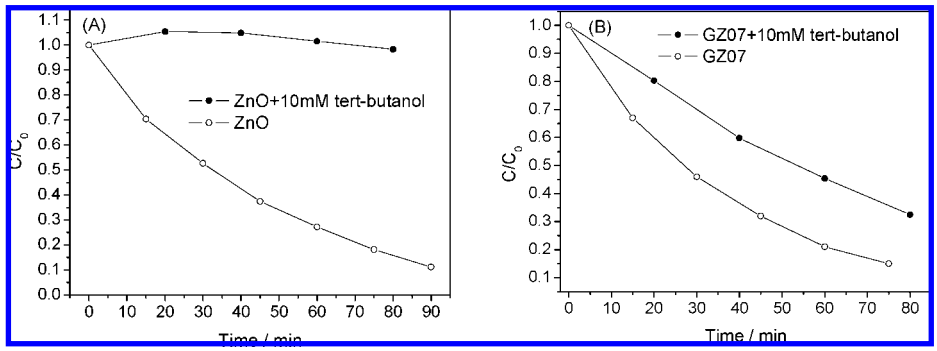

Figure 14. Effect of *tert*-butyl alcohol addition on the photodegradation of MB: (A) ZnO and (B) GZ07.

tocatalytic activities at low and high pH values can be attributed to the dissolution in strong acidic or alkaline environment.

In present work, the original ZnO nanoparticles are extremely susceptive to facile dissolution at extreme pH values. It follows that particular attention should be paid to the control of pH for practical applications. For GZ samples, the carbon shell, which could protect GZ samples against corrosion, results in a weaker pH dependence of the photocatalytic efficiency, as opposed to the case of ZnO.

3.4. Photocorrosion Suppression. To evaluate the photostability of the catalyst, the recycled experiments for the photodegradation of MB were performed, and the results are shown in Figure 11. When ZnO was used for the first time, 85% of MB could be degraded. After 12 h of photocatalytic reaction, a significant decrease of photocatalytic activity for pure ZnO was found (Figure 11A), the reaction rate constant decreased from 0.0172 min^{-1} to 0.0076 min^{-1}, namely, only 40% of MB was degraded for 80 min. After exposure under UV light for 96 h, photocatalytic degradation of MB was hardly evident, with a reaction rate of 0.0022 min^{-1}, which is only one-eighth of the initial reaction rate (0.0172 min^{-1}). Interestingly, after ZnO photocatalyst was surface hybridized with graphite-like carbon layers, long photocatalytic reaction times did not affect the photocatalytic activity apparently (Figure 11A). Even after irradiation under UV light for a month, more than 70% the photocatalytic activity of the initial GZ07 was preserved (Figure 11B). The drastic decrease of photocatalytic activity for ZnO was related to the photocorrosion effect. Apparently, the photocorrosion effect of ZnO was inhibited after surface hybridized by carbon layers.

The morphologies of the samples after photocatalysis were also observed, shown in Figure 12. After the 96 h of photocatalysis reaction, big web-like morphologies with sizes of hundreds nanometers were readily observed, instead of the original spherical ZnO particles, indicating that the structure of the ZnO crystal has been destroyed. Amazingly, in the presence of the carbon layers, the morphology of ZnO was well preserved (Figure 12B). To understand the morphology change during the photocatalysis reaction, the web-like substance was further investigated by XRD. The results are shown in Figure 13. For pure ZnO, after 96 h of photocatalysis reaction, new diffraction peaks appeared at 12.8°, 27.9°, 32.8°, and 60.1°, which could be assigned to the $Zn_5(OH)_6(CO_3)_2$ phase, suggesting that the crystal structure of ZnO was destroyed. However, the XRD pattern of the carbon layer encapsulated ZnO varied negligibly after long photocatalysis times. Therefore, the presence of carbon layers on the surface could significantly enhance the stability of ZnO nanoparticles during photocatalysis reaction.

3.5. Proposed Mechanism of Photocorrosion Suppression. In the photocatalysis process, the semiconductor is excited with UV light of wavelengths less than 380 nm to produce conduction band electrons and valence band holes which are capable of initiating photoreduction and photooxidation reactions, respectively.

$$ZnO + h\nu \rightarrow ZnO(e^- \cdots h^+) \quad (1)$$

For photooxidations occurring in oxygenated, aqueous media, the mechanism may, furthermore, involve direct reaction of the organic chemical (dye) with h^+, indirect reaction with trapped holes also described as adsorbed or surface-bound hydroxyl radicals, or a dual mechanism involving both surface holes and radicals.

$$h^+/OH^\bullet + \text{dye (MB)} \rightarrow \text{products} \quad (2)$$

To differentiate between direct photooxidation of MB by reaction with h^+ or indirect photooxidation via reaction with $OH^\bullet$ radicals, experiments were carried out by adding *tert*-butyl alcohol to minimize the formation of $OH^\bullet$ radicals. The results are shown in Figure 14. It is very interesting to see from Figure 14A that MB could hardly be degraded in the presence of ZnO when 10 mM *tert*-butyl alcohol was added, indicating that oxidation was proceeding by reaction with $OH^\bullet$ radicals. However, for the sample of GZ07, although the reaction rate was decreased, MB was still efficiently degraded in the presence of $OH^\bullet$ radical scavenger (Figure 14B). Therefore, a dual mechanism involving both surface holes and radicals is expected in the photocatalysis process of GZ07 sample. On the basis of the above results, it can be seen that the encapsulation of carbon layers changed the photocatalysis process of ZnO. In the case of bare ZnO, photoreactions occurred mainly in the bulk solution via reacting with $OH^\bullet$ radicals. For carbon capsulated ZnO, the photoreactions occurred both on the surface via direct reaction with h^+ and in the bulk solution. This difference could be attributed to the remarkably enhanced adsorption of MB on the surface as ZnO was coated by carbon layers. It has been reported that some reactions can be initiated by direct hole oxidation, especially when the adsorption by the substrates is rather extensive and the concentrations of substrates are relatively high.[27,28] The presence of carbon layers could gather the MB molecules on the surface of ZnO, which would facilitate the direct reaction of MB with surface holes h^+. Thus, MB could be efficiently photodegraded by GZ07 even in the presence of $OH^\bullet$ radical scavenger.

In the past, there was much evidence to suggest that the ZnO semiconductor suffers from the photoinduced dissolution, which greatly decreases its photocatalytic activity.[29] This photocorrosion process of the ZnO semiconductor can be represented by

$$ZnO + 2h^+ + nH_2O \rightarrow Zn(OH)n^{(2-n)+} + 0.5O_2 + nH^+ \quad (3)$$

where n depends on the pH of the solution. According to Gerischer's report, the sequence of steps involved in the

photodecomposition of ZnO crystals consists of two slow steps where two holes are trapped on the surface, followed by the fast formation of an oxygen molecule and the fast expulsion of Zn^{2+} from the surface,[30] i.e.

$$O^{2-}{}_{surface} + h^+ \rightarrow O^-{}_{surface} \quad (4)$$

$$O^-{}_{surface} + 3O^{2-} + 3h^+ \rightarrow 2(O-O^{2-}) \quad (5)$$

$$O-O^{2-} + 2h^+ \rightarrow O_2 \quad (6)$$

$$2Zn^{2+} \rightarrow 2Zn^{2+}(aq) \quad (7)$$

The overall reaction may be represented as

$$ZnO + 2h^+ \rightarrow Zn^{2+} + 0.5O_2 \quad (8)$$

In the present study, the nanosized ZnO particles suffered serious photocorrosion during the photocatalysis process. Inevitably, the photocatalytic activity was significantly decreased, and even the morphology and composition of the nanoparticles were changed. However, as the nanoparticles were capsulated with carbon layers, the photocorrosion was efficiently suppressed, and the stability was also significantly improved. The reasons are then proposed as follows:

First, based on eqs 2 and 8, it is known that the photoinduced dissolution and photocatalytic reaction are two competition processes. For pure ZnO nanoparticles, when exposed to UV irradiation, most of the generated h^+ would participate in the reaction of photocorrosion (eq 8). As the surface of ZnO was capsulated by carbon layers, due to the strong adsorption of MB molecules, part of the photogenerated h^+ was consumed in the photooxidation of MB (eq 2), which would compete with the photocorrosion process, and significantly suppress the serious photoinduced dissolution. Second, surface effects and small-size effects are characteristics of nanometer-sized particles, thus, nanosized ZnO particles suffered very serious photocorrosion. So, it is not surprising to see that the morphology of ZnO nanoparticles was changed and further formed a web-like structure during the photocatalysis process. Once the surface was coated by carbon layers, the surface reaction between ZnO particles will be inhibited, and the carbon layer will become a firm barrier against the formation of web-like structure. Finally, it is important to note that the crystal structure of ZnO in GZ samples is greatly enhanced due to the high temperature calcinations, which will also remarkably increase the stability of ZnO nanoparticles.

4. Conclusion

The presence of carbon layers could significantly suppress the photocorrosion of ZnO under the UV light irradiation, as well as the susceptibility of ZnO to facile dissolution at extreme pH values. The nanosized structure of ZnO was well preserved even after high-temperature calcination due to the carbon layers shell. The photocatalytical activity of ZnO can also be improved due to the enhanced adsorption ability and suppressed crystal growth. The graphite-like carbon coating is proven to be a promising approach to develop highly efficient and stable ZnO photocatalysts.

Acknowledgment. This work is supported by the National Natural Science Foundation of China (20673065) and the National Basic Research Program of China (2007CB613303).

References and Notes

(1) Hoffmann, M. R.; Martin, S. T.; Choi, W.; Bahnemann, D. W. *Chem. Rev.* **1995**, *95*, 69.
(2) M, A. Fox; Dulay, T. *Chem. Rev* **1995**, *95*, 735.
(3) Hariharan, C. *Appl. Catal., A* **2006**, *304*, 55.
(4) Richard, C.; Bosquet, F.; Pilichowski, J. F. *J. Photochem. Photobiol. A* **1997**, *108*, 45.
(5) Driessen, M. D.; Miller, T. M.; Grassian, V. H. *J. Mol. Catal. A: Chem.* **1998**, *131*, 149.
(6) Yeber, M. C.; Rodrýguez, J.; Freer, J.; Durian, N.; Mansilla, H. D. *Chemosphere* **2000**, *41*, 1193.
(7) Percherancier, J. P.; Chapelon, R.; Pouyet, B. *J. Photochem. Photobiol. A* **1995**, *87*, p. 261.
(8) Gouvea, K.; Wypych, F.; Moraes, S. G.; Duran, N.; Nagata, N.; Peralta-Zamora, P. *Chemosphere* **2000**, *40*, 433.
(9) Dindar, S.; Icli, J. *J. Photochem. Photobiol. A: Chem.* **2001**, *140*, 263.
(10) Kamat, P. V.; Huehn, R.; Nicolaescu, R. *J. Phys. Chem. B* **2002**, *106*, 788.
(11) Rao, M. V.; Rajeshwar, K.; Verneker, V. R. P.; DuBow, J. *J. Phys. Chem.* **1980**, *84*, 1987.
(12) Meulenkamp, E. A. *J. Phys. Chem. B* **1998**, *102*, 7764.
(13) Spathis, P.; Poulios, I. *Corros. Sci.* **1995**, *37*, 673.
(14) van Dijken, A.; Janssen, A. H.; Smitsmans, M. H. P.; Vanmaekelbergh, D.; Meijerink, A. *Chem. Mater.* **1998**, *10*, 3513.
(15) Wang, H. C.; Liu, P.; Wang, S. M.; Han, W.; Wang, X. X.; Fu, X. Z. *J. Mol. Catal. A: Chem.* **2007**, *273*, 21.
(16) Jongh, P. E.; Meulenkamp, E. A.; Vanmaekelbergh, D.; Kelly, J. J. *J. Phys. Chem. B* **2000**, *104*, 7686.
(17) Daneshvar, N.; Salari, D.; Khataee, A. R. *J. Photochem. Photobiol. A* **2004**, *162*, 317.
(18) Comparelli, R.; Fanizza, E.; Curri, M. L.; Cozzi, P. D.; Mascolo, G.; Agostiano, A. *Appl. Catal., B* **2005**, *60*, 1.
(19) Shanmugam, S.; Gabashvili, A.; Jacob, D. S.; Yu, J. C.; Gedanken, A. *Chem. Mater.* **2006**, *18*, 2275.
(20) Zhang, L. W.; Fu, H. B.; Zhu, Y. F. *Adv. Funct. Mater.* **2008**, *18*, 2180–2189.
(21) Inagaki, M.; Hirose, Y.; Matsunaga, T.; Tsumura, T.; Toyoda, M. *Carbon* **2003**, *41*, 2619.
(22) Sobana, N.; Muruganandam, M.; Swantinathan, M. *Catal. Commun.* **2008**, *9*, 262.
(23) Sobana, N.; Swaminathan, M. *Sol. Energy Mater. Sol. Cells* **2007**, *91*, 727.
(24) Eklund, P. C.; Holden, J. M.; Jishi, R. A. *Carbon* **1995**, *33*, 959.
(25) Su, F. B.; Zhao, X. S.; Wang, Y.; Zeng, J. H.; Zhou, Z. C.; Lee, J. Y. *J. Phys. Chem. B* **2005**, *109*, 20200.
(26) Tuinstra, F.; Koenig, J. L. *J. Chem. Phys.* **1970**, *53*, 1126.
(27) Kim, S.; Park, H.; Choi, W. *J. Phys. Chem. B* **2004**, *108*, 6402.
(28) Zhu, S. B.; Xu, T. G.; Fu, H. B.; Zhao, J. C.; Zhu, Y. F. *Environ. Sci. Technol.* **2007**, *41*, 6234.
(29) Spathis, P.; Poulio, I. *Corros. Sci.* **1995**, *51*, 673.
(30) Rudd, A. L.; Breslin, C. B. *Electrochim. Acta* **2000**, *45*, 1571.

JP807778R